

Application of deformation-induced topographic effect in interpretation of 2013–2016 spatiotemporal gravity changes at Laguna del Maule (Chile)

Peter Vajda^{a,*}, Pavol Zahorec^a, Craig A. Miller^b, H el ene Le M evel^c, Juraj Pap čo^d, Antonio G. Camacho^e

^a Earth Science Institute, Slovak Academy of Sciences, D ubravsk a cesta 9, P.O.Box 106, SK-840 05, Bratislava, Slovakia

^b GNS Science, Wairakei Research Center, Private Bag 2000, Taup o 3330, New Zealand

^c Carnegie Institution for Science, Earth and Planets Laboratory, 5241 Broad Branch Road NW, Washington, DC 20015, USA

^d Dept. of Theoretical Geodesy and Geoinformatics, Slovak University of Technology, Radlinsk eho 11, SK-810 05 Bratislava 15, Slovakia

^e Institute of Geosciences (CSIC-UCM), C/Doctor Severo Ochoa, 7, Ciudad Universitaria, 28040, Madrid, Spain

*Corresponding author: Peter.Vajda@savba.sk, ORCID: 0000-0001-9046-480X, SCOPUS ID: 7005183079

Session G4.4 EGU21-467 <https://doi.org/10.5194/egusphere-egu21-467>

Deformation induced effects in residual gravity change computation

Spatiotemporal (time-lapse) gravity changes observed in volcanic areas are complex composite signals. The observed gravity changes (Δg) must be first corrected for all signal components other than those associated with the studied volcanic processes. Among these are atmospheric and tidal effects, instrumental and survey design effects, and hydrological effects. If elevation changes, i.e. surface vertical displacements (Δh), accompany gravity changes then the gravitational effect of the surface deformation must be carefully accounted for. To extract the gravitational signal component respective only to the mass and/or density changes related to the source (Δg^M), several gravitational effects must still be removed. This removal of unwanted signal components constitutes the computation of residual gravity changes Δg^{res} :

$$\Delta g^{\text{res}}(P) \equiv \Delta g(P) - \Delta g^{\text{FAE}}(P) - \Delta g^{\text{sdef}}(P) - \Delta g^{\text{idef}}(P) = \Delta g^M(P). \quad (1)$$

The individual signal components, evaluated at the gravity benchmark on the (post-deformation) topographic surface (P) are as follows. The Δg^{FAE} term is the so called *free-air effect* (FAE). It is the gradient effect based on the true (in situ) *vertical gradient of gravity* (VGG). The FAE is due to the vertical displacement of the gravity benchmark in the ambient gravity field, i.e. in free-air, disregarding the fact that the topographic masses attached to the deformed surface are moving along with the displaced surface. The latter effect is treated as the attraction of surface deformation (Δg^{sdef}). The Δg^{sdef} term is the attraction of topographic masses enclosed between the pre- and post-deformation topographic surfaces. Due to the relief of the topographic surface, it must be numerically evaluated by 3D Newtonian volumetric integration. The Δg^{sdef} term may contain also the attraction of surface mass changes (such as outpoured lava flows, dome collapse or growth, accumulated fall-out products, flank collapse, lahars, etc.). The Δg^{idef} term is the attraction of inner deformations. While the attraction of surface deformation (Δg^{sdef}) can be computed from the observable surface deformation, and applied as a correction to observed gravity changes, the attraction of inner deformations can only be estimated or modelled.

The terms Δg^{FAE} and Δg^{sdef} should never be treated numerically separately. The reason is that both terms contain a highly variable short-wavelength signal due to the relief of the topographic surface, and their sum should be treated as one term, which was named the deformation-induced topographic effect (DITE)

$$\Delta g^{\text{DITE}}(P) \equiv \Delta g^{\text{FAE}}(P) + \Delta g^{\text{sdef}}(P). \quad (2)$$

The free-air effect (FAE) is based on the VGG (Γ) observed at the benchmark, by which the elevation change (Δh) of a benchmark is multiplied

$$\Delta g^{\text{FAE}}(P) = \Gamma(P)\Delta h(P). \quad (3)$$

The second DITE constituent (Δg^{sdef}), the attraction of surface deformation must be computed by a 3D Newtonian volumetric integration. The conceptual expression of DITE, [eq. \(2\)](#), is not well suited for the numerical evaluation of DITE, as it demands the measurement of VGG at each benchmark, which is not always possible. [Vajda et al. \(2019\)](#) have derived an expression for the DITE defined by [eq. \(2\)](#), which does not require the real VGG at benchmarks:

$$\Delta g^{\text{DITE}}(P) = \Gamma_0 \Delta h(P) + [a^{\text{T*}}(P^*) - a^{\text{T}}(P)] . \quad (4)$$

This new expression replaces the use of VGG in DITE by the use of the constant gradient of normal gravity (Γ_0). In this alternate DITE formula, the first term is a gradient effect, this time based on the constant theoretical (normal) free-air gradient (FAG), Γ_0 ($\Gamma_0 = -308.6 \mu\text{Gal/m}$, $1 \mu\text{Gal/m} = 10^{-8} \text{ s}^{-2}$). The square brackets term constitutes the difference between the attraction of the post-deformation topographic masses evaluated on the post-deformation topographic surface ($a^{\text{T*}}(P^*)$) and the attraction of the pre-deformation topographic masses evaluated on the pre-deformation topographic surface ($a^{\text{T}}(P)$). This is not the same as the attraction of masses trapped between pre- and post-deformation surfaces. The topographic masses are those bound between sea level and the earth surface. A constant reference density (ρ_0) of the topographic masses is adopted in evaluating this term. The square brackets term is evaluated by numerical volumetric Newtonian integration, which requires an accurate and high-resolution digital elevation model (DEM) of the study area, ideally with horizontal resolution less than 10 m and vertical accuracy better than 10 cm, a correct choice of the topographic reference density (ρ_0), and the availability of the vertical displacement field in areal form.

If the vertical displacements are only available as scattered point data at gravity benchmarks, then the DITE can be evaluated only approximately by multiplying the elevation change at each benchmark by some sort of gravity gradient value. The question arises which gradient value is to be used. Should one use in-situ VGG measured at each benchmark, or, if not available, its approximation by topographically-predicted VGG (e.g. [Vajda et al., 2020](#))? Should the constant theoretical (normal) FAG be used, or the Bouguer-corrected FAG (BCFAG)? Or do different conditions or situations require the use of different values of the vertical gradient? [Vajda et al. \(2019\)](#) addressed this question by performing numerical simulations of the DITE respective to various size and shape deformation fields imposed over relief features of various shapes. The outcome of their study is that most commonly the Bouguer approximation (BCFAG-DITE) would perform the best. It uses the planar BCFAG (Γ_B), cf. (e.g., [Berrino et al., 1984, 1992; Rymer, 1994](#)),

$$\Delta g^{\text{DITE}}(P) \approx \Gamma_B \Delta h(P) , \quad \text{where } \Gamma_B = [\Gamma_0 + 2\pi G\rho_0] , \quad (5)$$

where G is the Newton constant and Γ_0 is the constant theoretical FAG. However, under particular conditions the “normal Free-Air Effect” (nFAE)

$$\Delta g^{\text{DITE}}(P) \approx \Gamma_0 \Delta h(P) \quad (6)$$

becomes a better approximation of DITE. Numerical simulations revealed that the physical nature of DITE varies between two limiting cases: the nFAE-DITE and the BCFAG-DITE. The DITE varies depending on the shape, lateral extent and amplitude of the deformation field, as well as the shape of the relief over which it is imposed. In flatter or less rugged relief the nature of DITE is closer to its Bouguer representation ([eq. \(5\)](#)). In special cases of short-wavelength deformation fields (such as those generated by shallow small spherical sources or by vertically elongated shallow sources) imposed over steep cone-shape terrain the nature of DITE is closer to its normal-free-air representation ([eq. \(6\)](#)).

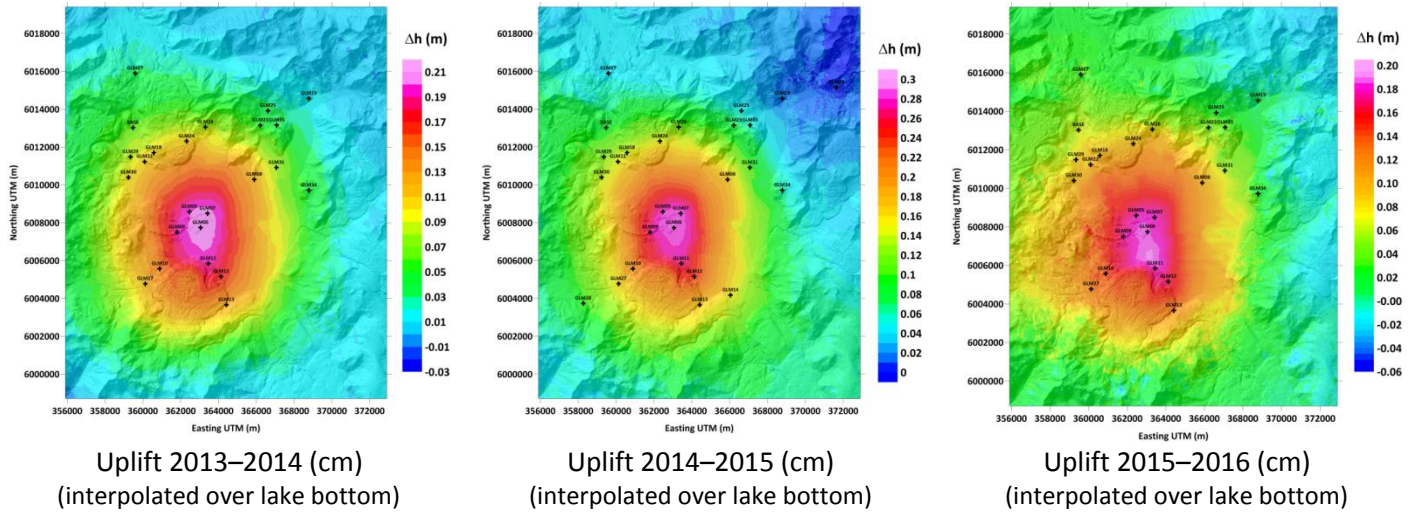
To reduce the observed gravity changes for the effect of the uplift, i.e., for the effect of elevation changes at gravity benchmarks, [Miller et al. \(2017\)](#) used at the LdMvf a constant value of the gradient on all benchmarks of the gravimetric network,

$$\Delta g^{\text{DITE}}(P) \approx \Gamma_L \Delta h(P) . \quad (7)$$

The constant local gradient was determined by in-situ measurements at a reference benchmark as $\Gamma_L = -335 \pm 4 \mu\text{Gal/m}$. The effect of this correction on the resulting data inversion and interpretation will be examined numerically by our case study presented below. In [section 3.2](#) we compare the DITE computed by [eq. \(4\)](#) with the effect computed using [eq. \(7\)](#) at the LdMvf.

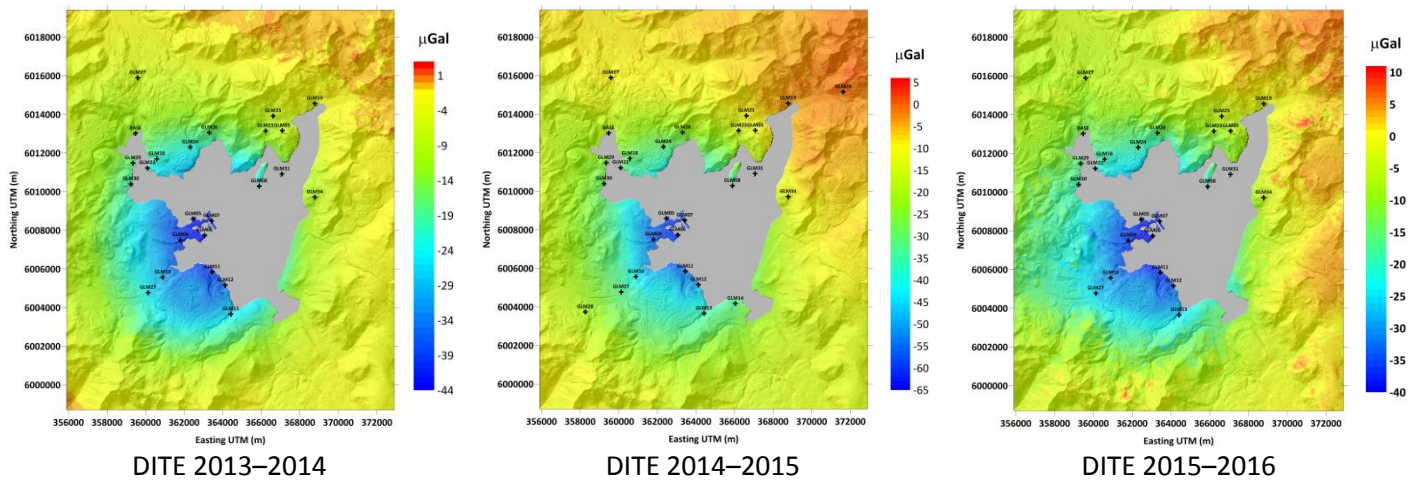
Deformation at Laguna del Maule volcanic field

The LdMvf is situated within the Andean Southern Volcanic zone. Since 2007, widespread deformation at rates greater than 20 cm/year (Feigl et al., 2014; Le Mével et al., 2015, 2016) has been observed and modeled as an inflating sill (Zhan et al., 2019) at about 5 km depth (below surface, i.e., 3 km below sea level).



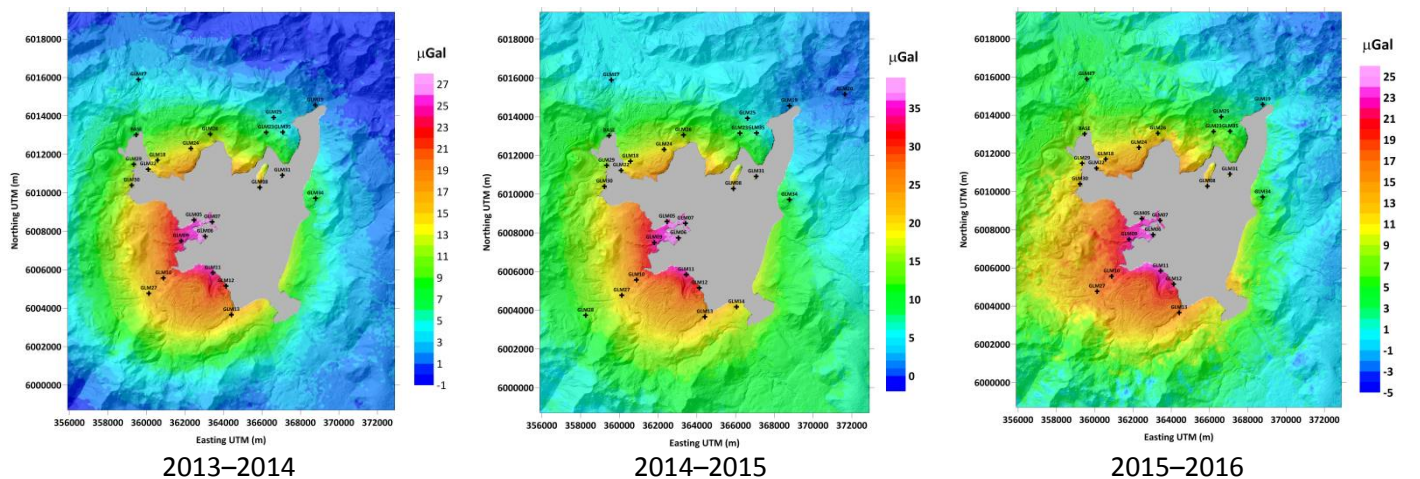
DITE respective to deformation at LdMvf

The DITE field (μGal) is computed using volumetric integration (eq. (4)) and software Toposk (Zahorec et al. 2017)



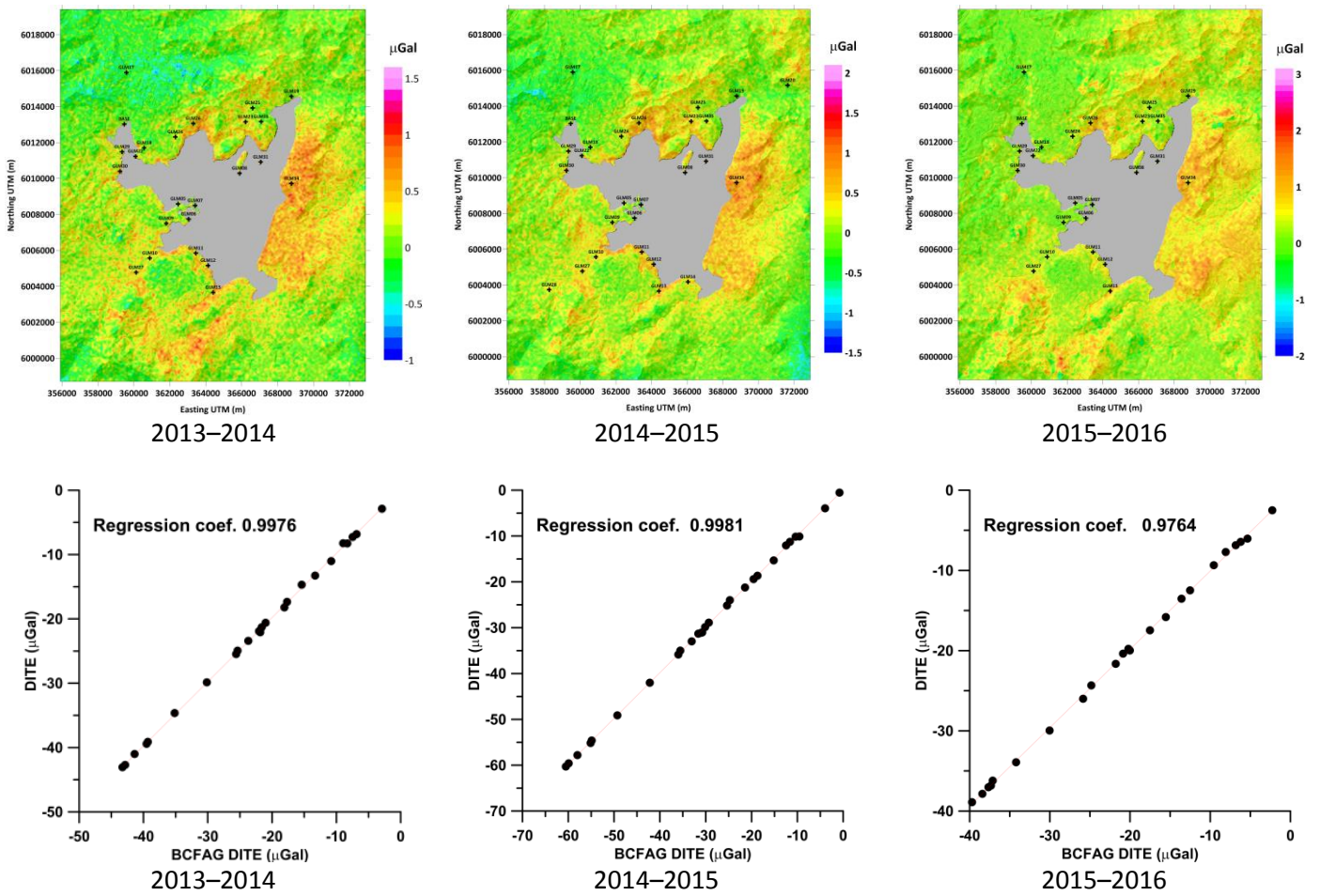
Difference between DITE and local FAE respective to deformation at LdMvf

The difference between the DITE field (μGal), computed using Newtonian volumetric integration (eq. (4)) and the local FAE field (eq. (7)) for $\Gamma_L = -335 \pm 4 \mu\text{Gal/m}$.



Bouguer approximation of DITE
Difference between DITE field and its Bouguer approximation DITE respective to deformation at LdMvf

The difference between the DITE field (μGal), computed using Newtonian volumetric integration (eq. (4)) and its Bouguer approximation (eq. (6))



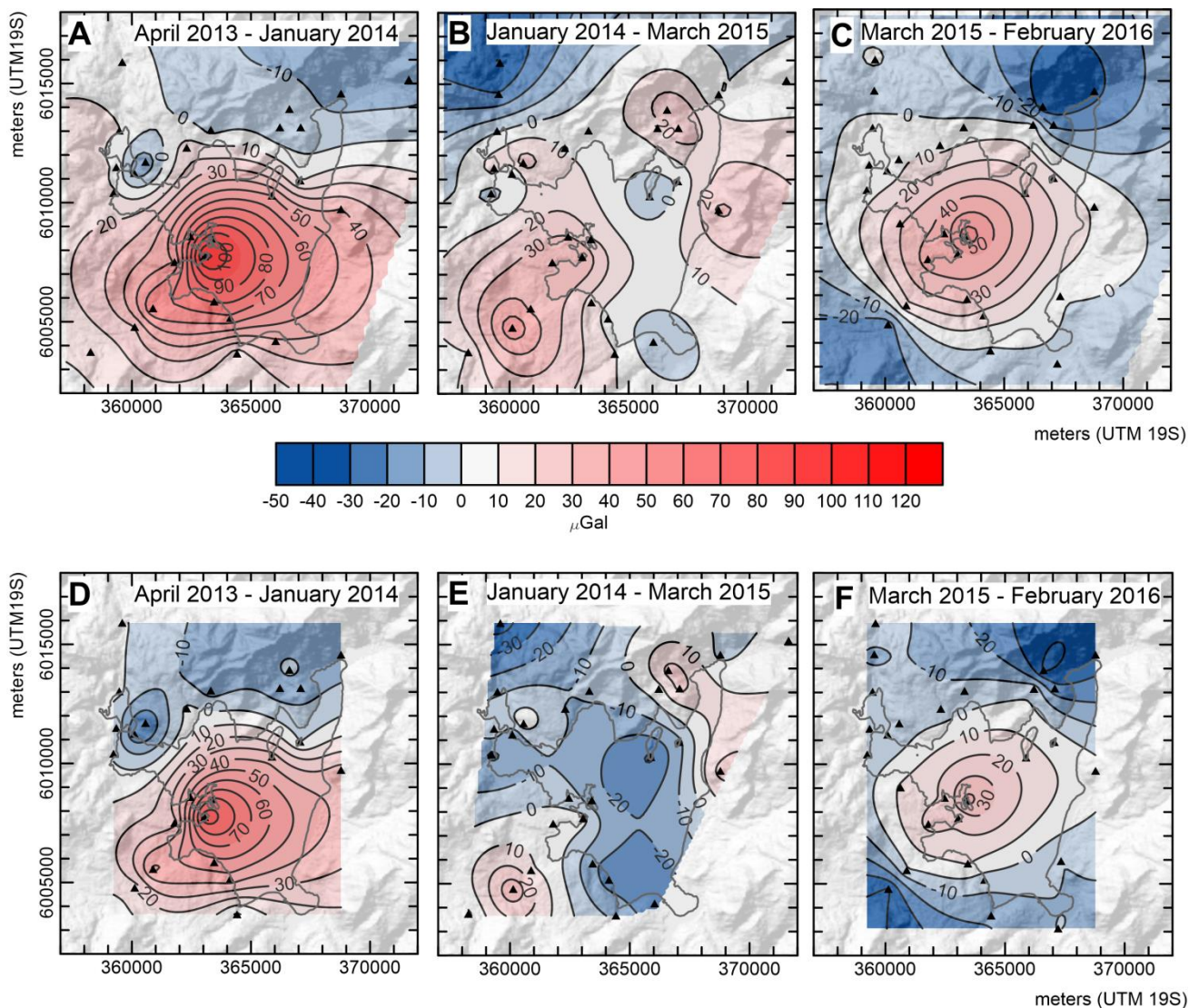
The statistics of the differences between the DITE and the Bouguer approximation of DITE (BCFAG-DITE) in (μGal) computed at benchmarks

period	min(abs)	max(abs)	mean	rms
2013–2014	0.0	0.7	+0.2	0.3
2014–2015	0.0	0.7	+0.2	0.3
2015–2016	0.0	0.9	-0.1	0.4

At a site with terrain morphology like that at LdMvf and a deformation field alike the one at LdMvf (widespread and monotonous), the DITE can be adequately (accurately) approximated by its planar Bouguer representation.

**Residual gravity changes at benchmarks
DITE-corrected vs local-FAE-corrected gravity changes at LdMvf**

Residual gravity changes at LdMvf computed for the three time intervals
(A–C) with the local FAE (using the $-335 \pm 4 \mu\text{Gal}/\text{m}$ gradient), and (D–F) with the DITE.
Gravity benchmarks are shown as black triangles and data are interpolated between benchmarks.



The statistics of the **differences** between the DITE-corrected and the local-FAE-corrected gravity changes (μGal) computed from benchmark values

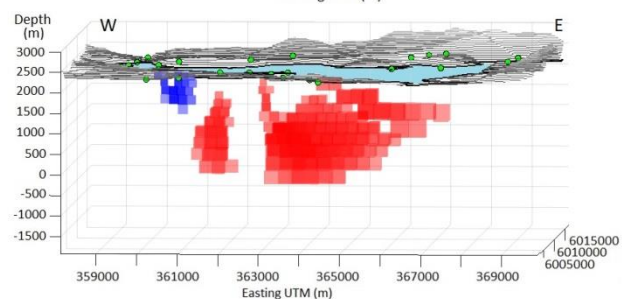
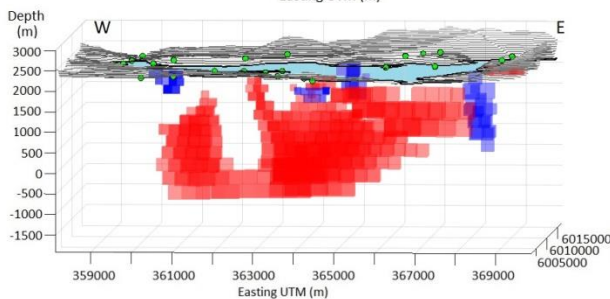
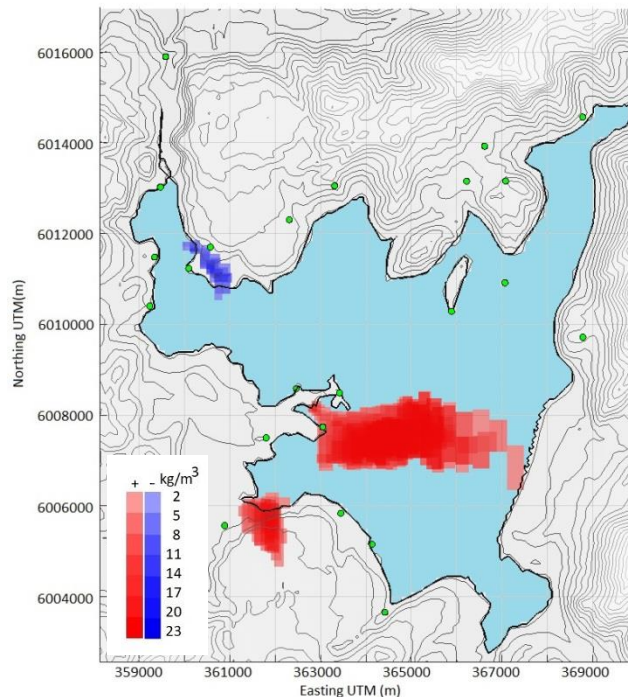
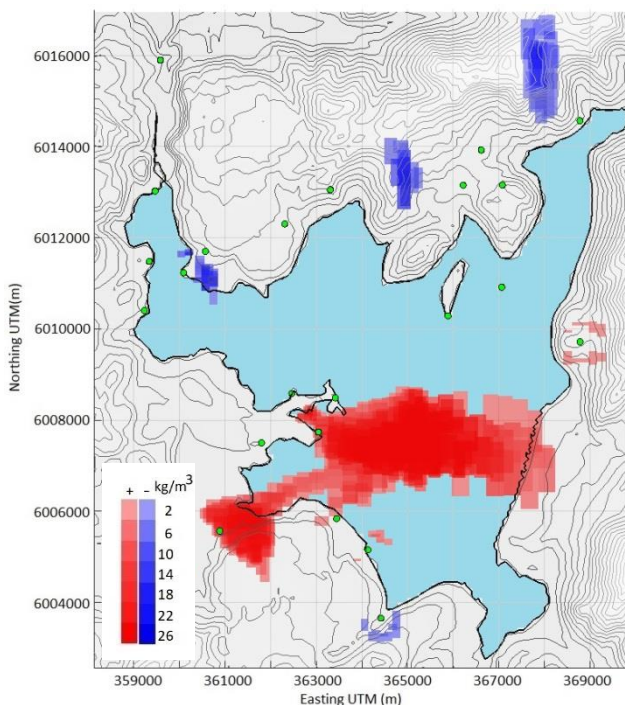
period	min(abs)	max(abs)	mean	rms
2013–2014	2	27	-14	16
2014–2015	1	37	-19	21
2015–2016	2	23	-13	14

**Genetic Algorithm (GA) inversion (for a vertical prism) of residual gravity changes at benchmarks
DITE-corrected vs local-FAE-corrected gravity changes at LdMvf**

The GA modelling of Miller et al. (2017) was repeated on the DITE-corrected gravity changes, solving for a vertical prism source. Strikes of the admissible prisms are similar but with larger scatter compared to the original inversion. The depth to the top of the prism is now shallower, 1350 m a.s.l., compared to the previous 500 m a.s.l. The mass of the prism is less, 7×10^{10} kg compared to 13×10^{10} kg, and the prism is now wider but has less depth extent (thickness). Overall, the source is still well aligned along the Troncoso and other faults that extend under the lake. Hence the interpretation of the source mechanism, the migration of fluids into the Troncoso fault, remains the same as in (Miller et al., 2017). However, the new interpretation requires less fluid transfer into the fault zone, with implications for hydrologic parameters such as permeability and hydraulic conductivity. For example, less fluid flux into the fault zone reduces the permeability estimate of the fault zone from 12×10^{-12} to $6.4 \times 10^{-12} \text{ m}^2$.

**Growth inversion of residual gravity changes at benchmarks
DITE-corrected vs local-FAE-corrected gravity changes at LdMvf**

Here we compare the Growth inversion (Camacho et al., 2011, 2021) results of gravity changes corrected by the local FAE eq. (7) to those corrected by the DITE (eq. (4)). Red indicates mass addition, blue indicates mass loss.

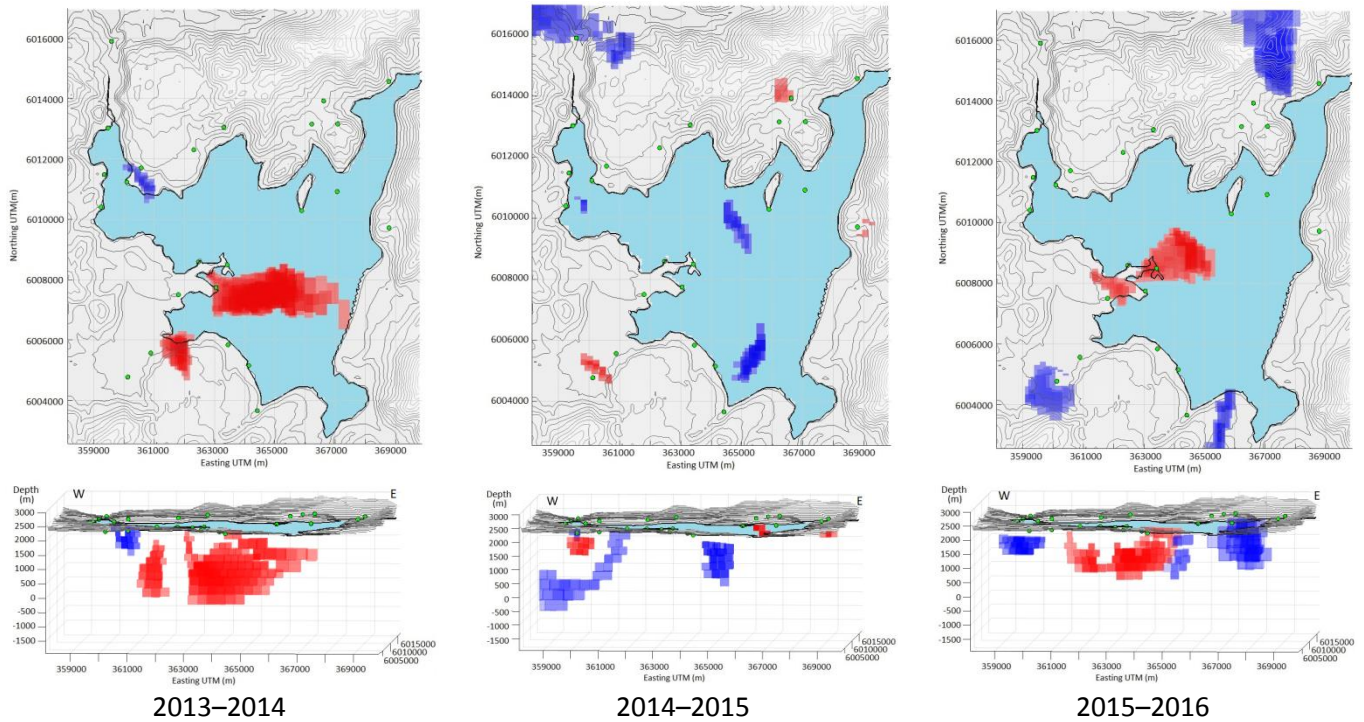


Growth model obtained from FAE-corrected gravity changes 2013–2014

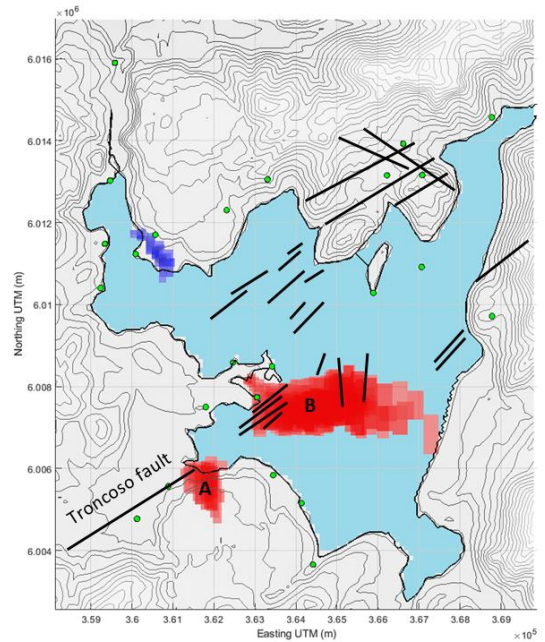
Growth model obtained from DITE-corrected gravity changes 2013–2014

The sources obtained for the DITE-corrected data are shallower, compared to the source body obtained for the FAE-corrected data, and contain altogether less mass. The average depth of the cells with positive differential density (mass addition) changed from 650 m a.s.l. to 860 m a.s.l. for FAE and DITE correction, respectively. Mass addition decreased from 18.7×10^{10} kg to 8.9×10^{10} kg. The replacement of the FAE correction by the DITE correction thus mainly affected the total mass change, but also the depth of the injected mass.

Growth inversion of DITE-corrected gravity changes over the 3 periods



The periods 2013–14 and 2015–16 exhibit a similar pattern of fluid input. The mass addition is mainly located in the central part of the lake Maule, where the Troncoso and other vertical dip-slip faults serve as pathways for fluid migration. The 2014–2015 solution shows small regions of mass loss rather than mass input. This time interval represents a pause in the process of mass addition along the Troncoso fault. Such cyclicity in mass changes was modeled by [Zhan et al. \(2019\)](#) as a process of fault zone dilation caused by sill inflation. High pressure fluid from around the magma reservoir injects into the dilatant fault zone triggering seismicity. The fluid migrates to unsaturated shallow storage regions creating the positive gravity anomaly. The pore pressure around the fault zone will then decrease, stopping seismicity and closing the fault zone to mass addition until the next cycle of magmatic fluid release. This effect becomes more pronounced in the DITE corrected gravity data compared to the FAE corrected data, where some small gravity change was observed in the 2015–2016 period. Regions of mass loss in 2014–2016 that are close to the fault zones may indicate the sources of fluid that migrated laterally into the fault zones, however it is thought that most of the fluid migrates vertically as lateral mass loss is smaller than the mass addition. Mass loss regions further from the fault zone may reflect seasonal aquifer changes.



Highlights

- accurate DITE correction to be used for computing residual 4D micro-gravity changes
- impact of not using DITE on inversion and interpretation illustrated by case study
- Bouguer approximation of DITE shown accurate in less rugged areas
- Growth inversion tool applied to sparse scattered inaccurate 4D micro-gravity data

References

- Berrino, G., Corrado, G., Luongo, G., Toro, B., 1984. Ground deformation and gravity changes accompanying the 1982 Pozzuoli uplift. *Bull. Volcanol.* 47, 187–200
- Berrino, G., Rymer, H., Brown, G.C., Corrado, G., 1992. Gravity-height correlations for unrest at calderas. *J. Volcanol. Geotherm. Res.* 53, 11–26
- Camacho, A., Fernández, J., Gottsmann, J., 2011. The 3-D gravity inversion package GROWTH 2.0 and its application to Tenerife Island, Spain. *Computers & Geosciences* 37, 4, 621–633, doi 10.1016/j.cageo. 2010.12.003
- Camacho, A.G., J.F. Prieto, A. Aparicio, E. Ancochea, J. Fernández, 2021. Upgraded GROWTH 3.0 software for structural gravity inversion and application to El Hierro (Canary Islands). *Computers and Geosciences* vol.150, <https://doi.org/10.1016/j.cageo.2021.104720>
- Feigl, K.L., Le Mével, H., Tabrez Ali, S., Cordova, L., Andersen, N.L., DeMets, C., Singer, B.S., 2014. Rapid uplift in Laguna del Maule volcanic field of the Andean Southern Volcanic zone (Chile) 2007–2012. *Geophys. J. Int.* 196(2), 885–901, doi:10.1093/gji/ggt438
- Le Mével, H., Feigl, K.L., Córdoba, L., DeMets, C., Lundgren, P., 2015. Evolution of unrest at Laguna del Maule volcanic field (Chile) from InSAR and GPS measurements, 2003 to 2014. *Geophys. Res. Lett.* 42, 6590–6598, doi:10.1002/2015GL064665
- Le Mével, H., Gregg, P.M., Feigl, K.L., 2016. Magma injection into long-lived reservoir to explain geodetically measured uplift: Application to the 2004–2015 episode at Laguna del Maule volcanic field, Chile. *J. Geophys. Res. Solid Earth* 121, 6092–6108, doi:10.1002/2016JB013066
- Miller, C.A., Le Mével, H., Currenti, G., Williams-Jones, G., Tikoff, B., 2017b. Microgravity changes at the Laguna del Maule volcanic field: Magma-induced stress changes facilitate mass addition. *J. Geophys. Res. Solid Earth*, 122, doi:10.1002/2017JB014048.
- Rymer, H., 1994. Microgravity change as a precursor to volcanic activity. *J. Volcanol. Geotherm. Res.* 61, 311–328
- Vajda, P., Zahorec, P., Bilčík, D., Papčo, J., 2019. Deformation-induced topographic effects in interpretation of spatiotemporal gravity changes: Review of approaches and new insights. *Surv. Geoph.* 40, 1095–1127, doi 10.1007/s10712-019-09547-7
- Vajda, P., Zahorec, P., Papčo, J., Carbone, D., Greco, F., Cantarero, M., 2020. Topographically predicted vertical gravity gradient field and its applicability in 3D and 4D microgravimetry: Etna (Italy) case study. *Pure and Applied Geophysics*, 177(7): 3315–3333, <https://doi.org/10.1007/s00024-020-02435-x>
- Zahorec, P., Marušiak, I., Mikuška, J., Pašteka, R., Papčo, J., 2017. Numerical Calculation of Terrain Correction Within the Bouguer Anomaly Evaluation (Program Toposk), chapter 5, 79–92. In book: Pašteka, R., Mikuška, J., Meurers, B. (eds.): *Understanding the Bouguer Anomaly: A Gravimetry Puzzle*, Elsevier, ISBN 978-0-12-812913-5, doi 10.1016/B978-0-12-812913-5.00006-3
- Zhan, Y., Gregg, P.M., Le Mével, H., Miller, C.A., Cardona, C., 2019. Integrating reservoir dynamics, crustal stress, and geophysical observations of the Laguna Del Maule magmatic system by FEM models and data assimilation. *Journal of Geophysical Research: Solid Earth*, 124, 13547–13562. Doi /10.1029/ 2019JB018681

Acknowledgments

P.V. was supported by the Slovak Research and Development Agency under the contract (project) No. APVV-16-0482 (acronym LITHORES) and by the VEGA grant agency under project No. 2/0006/19. P.Z. and J.P. were supported by the Slovak Research and Development Agency under the contract (project) No. APVV-19-0150 (acronym ALCABA) and the VEGA grant agency under project 2/0100/20. H.L.M. acknowledges SAR data from ESA (Sentinel-1) and DLR (TerraSAR-X). H.L.M. thanks JPL for distributing the ISCE software and Yunjun Zhang for helpful discussions on time series analysis with MintPy. We thank OVDAS for their support in maintaining the GPS network at LdMvf and sharing GPS data. We also thank Angie Diefenbach for providing the high resolution DEM of LdMvf. The LdMvf project was funded by NSF EAR-1411779. C.A.M. is supported by the New Zealand government MBIE funded GNS Science Volcanic Hazards Programme. A.G.C. has been supported by the Spanish Ministerio de Ciencia, Innovación and Universidades research project DEEP-MAPS (RTI2018-093874-B-I00).